MULTISCALE MODEL. SIMUL.
Vol. 12, No. 1, pp. 335–363

ANALYSIS OF CONTROL VOLUME HETEROGENEOUS MULTISCALE METHODS FOR SINGLE PHASE FLOW IN POROUS MEDIA*

SERGEY ALYAEV†, EIRIK KEILEGAVLEN†, AND JAN MARTIN NORDBOTTEN†

Abstract. The standard approximation for the flow-pressure relationship in porous media is Darcy's law that was originally derived for infiltration of water in fine homogeneous sands. Ever since there have been numerous attempts to generalize it for handling more complex flows. Those include upscaling of standard continuum mechanics flow equations from the fine scale. In this work we present a heterogeneous multiscale method that utilizes fine scale information directly to solve problems for general single phase flow on the Darcy scale. On the coarse scale it only assumes mathematically justified conservation of mass on control volumes, that is, no phenomenological Darcy-type relationship for velocity is presumed. The fluid fluxes are instead provided by a fine scale Navier–Stokes mixed finite element solver. This work also considers several choices of quadrature for data estimation in the multiscale method and compares them. We prove that for an essentially linear regime, when the fine scale is governed by Stokes flow, our method converges to a rigorously derived homogenization solution—Darcy's law. Moreover the method gives the flexibility to solve problems with faster nonlinear flow regimes that is important in a number of applications, such as flows that may occur near wells and in fractured regions in subsurface. Those flows are also common for industrial and near surface porous media. The numerical examples presented in the paper verify the estimate and emphasize the importance of good data estimation.

Key words. control volume method, heterogeneous multiscale method, a priori estimate

AMS subject classifications. 76S05, 34E13, 35B45, 65N08, 74Q05, 74Q15

DOI. 10.1137/120885541

1. Introduction.

Flow in porous media models several physical phenomena of great practical importance, spanning flow in natural geological systems to anthropogenic materials such as fuel cells or human tissue. At the same time, the rigorous description of the continuum scale equations, here referring to the scale where the porous structure is not resolved, has remained elusive for all but the simplest systems. Spanning research from the engineering to applied sciences, it remains one of the fundamentally unresolved cross-disciplinary challenges.

At the porous scale, the governing equations are well understood as those of fluids and solids with appropriate interface conditions. In this setting, one may allow for multiple fluid phases, as well as deformation of the porous material. However, the challenging geometry of the pore space coupled with the large length scales required by applications prohibits the use of direct numerical simulation on this scale.

The first continuum scale description was brought by the experimental result known as Darcy's law valid for slow single phase flows in homogeneous media. In the theoretical setting, a long history of works have set out to establish continuum

*Received by the editors July 23, 2012; accepted for publication (in revised form) November 26, 2013; published electronically March 18, 2014. This work has been done as a result of the Special Semester on Multiscale Simulation and Analysis in Energy and the Environment (October 3–December 16, 2011) organized by RICAM (Johann Radon Institute for Computational and Applied Mathematics, Austrian Academy of Science) Linz, Austria. The research of the authors receives financial support from The Research Council of Norway under grant 180679.

http://www.siam.org/journals/mms/12-1/88554.html

†University of Bergen, Department of Mathematics, Postboks 7803, NO-5020 Bergen (Sergey.Alyaev@math.uib.no, Eirik.Keilegavlen@uib.no, Jan.Nordbotten@math.uib.no).

relationships based on derivations from the pore scale which validated and extended Darcy's law (see, e.g., [27, 11, 36, 25, 26, 14]). While in all these works the derivation of the continuum conservation principles is relatively straightforward, the closure relationships almost uniformly lack analytical treatment. Furthermore, as one considers more complex flows, the derivations become largely untenable and for some cases it is not possible to achieve full decoupling [26].

This has led to a situation where two scale models have gained increased attention as a way to handle potentially complex porous media systems. To some extent, this can be seen in the development of general frameworks for two-level couplings (see, e.g., [10, 20, 29, 13, 18]), but also particular implementations tailored to porous media (see, e.g., [37, 22, 32, 28, 16, 8, 15]). Of particular interest to us is the work related to implementation of the heterogeneous multiscale method (HMM) framework (such as [5, 16, 8, 15]).

In this communication, we give a more thorough description of a new way to implement the HMM framework in the setting of control volume discretizations for the continuum conservation equation that was introduced in [8], that we refer to as control volume heterogeneous multiscale method (CVHMM). Our approach takes advantage of the mathematically justified continuity equation on the coarse scale and uses the full solution of the Navier–Stokes equations on perforated domains at the pore scale to recover constitutive relations. Such design makes the method capable of handling single-phase flow in porous media for arbitrary flow rates, thus extending beyond the validity of Darcy's law. Of importance, in the limit of low flow rates, the classical results are recovered.

An alternative approach is discussed in the work of Chu et al. [16] (and [15] that extends it) where for local computation, pore network modeling is performed. Instead of having an extra procedure of deriving a pore network possessing the same properties as the actual pore structure we do simulations directly on the porous geometry, hence, avoiding errors caused by network reconstruction but paying the price of more expensive fine scale computations. For problems where the details of the pore geometry become important, e.g., for nonlinear flows or more general problems involving deformation of the porous geometry, the direct treatment of the pore space as presented herein will be more accurate than the idealized network approaches.

In this work we propose two choices of the quadrature points. The first one follows [6, 16] and mimics control volume finite element methods. The second novel choice is more in the spirit of classical flux approximation schemes, wherein it preserves harmonic averages at the coarse scale, and thus is more robust to material discontinuities.

We complement the new method with a priori convergence analysis for the essentially linear flows. Our analysis follows the layout suggested by E, Ming, and Zhang in [21] and later developed for a fully discrete finite element framework by Abdulle [4, 5]. Here it is specifically adapted to the particular setting of finite volume discretization, such as presented in [12]. Furthermore, our analysis departs from Abdulle in the particular grouping of error terms. The analysis also differs from most of the previous work since in our case we have different problem formulations on different scales.

The remainder of the paper is structured as follows: In the next section, the model problem is established. In section 3, we define the method. After putting some additional assumptions on the method in section 4, the proof of an a priori estimate for the linear regime is presented in section 5, followed by section 6 containing observations regarding extensions of the analysis to nonlinear cases. After numerical examples in section 7 the paper is concluded by section 8.

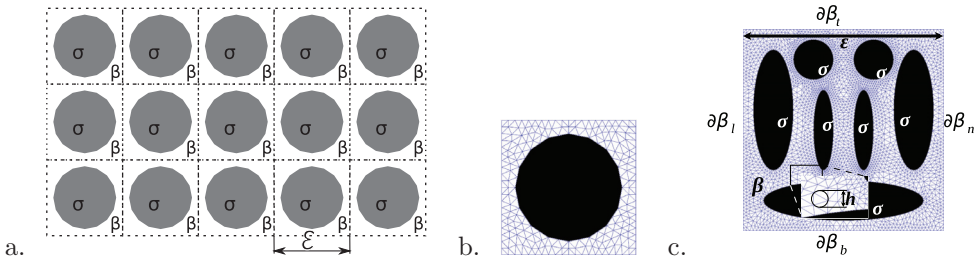

FIG. 1. *A simple periodic structure forming a coarse scale domain* (a) *and triangulation of a simple* (b) *and a more complex* (c) *cell problem.*

2. Model problem. The focus of this paper is the interplay between pore scale and Darcy scale. In this section we introduce model equations and briefly review a relation between the scales that can be derived by homogenization.

2.1. Model equations. On the pore scale the motion of fluids is governed by Navier–Stokes equations which for the incompressible case look as follows:

$$\nabla \cdot \vec{v}^{\varepsilon} = 0, \tag{2.1a}$$

$$\rho\left(\frac{\partial \vec{v}^{\varepsilon}}{\partial t} + \vec{v}^{\varepsilon} \cdot \nabla \vec{v}^{\varepsilon}\right) = -\nabla p^{\varepsilon} + \mu \nabla^2 \vec{v}^{\varepsilon} + \vec{f}. \tag{2.1b}$$

Here $\vec{v}^{\varepsilon}$ is fluid velocity, p^{ε} is the pressure associated with the fine scale (ε indicates the exact solution of the full fine scale problem), ρ is the constant fluid density, μ is viscosity, t is time and $\vec{f}$ is volumetric forces. These equations are valid in the pore volume inside the pore geometry the example of which is shown on Figure 1 and marked by β. Darker areas on Figure 1, marked by σ, represent the solid impermeable grains; in those areas and on their boundary there is no flow or

$$\vec{v}^{\varepsilon} = \vec{0}. \tag{2.2}$$

It is convenient to picture porous media as being combined of the "cells" of size ε as on Figure 1.

The coarse scale flux density $\vec{v}$ (defined as integrated velocity) is assumed to fulfill the continuity equation

$$\nabla \cdot \vec{v} = f, \tag{2.3}$$

where f is a source/sink term. Furthermore, we assume a relationship between the coarse pressure and flux density of the form

$$\vec{v}(\vec{x}) = \vec{F}(\nabla p(\vec{x}), \vec{x}). \tag{2.4}$$

We note that this formulation includes the well-known linear relation between the flux and the pressure gradient referred to as Darcy's law,

$$\vec{v} = -\frac{K}{\mu}\nabla p, \tag{2.5}$$

where the resistivity coefficient K is called the permeability. However the expression for $\vec{F}$ is more general as it also includes the cases of nonlinear relationships such as the Dupuit–Forchheimer–Ergun law.

2.2. Homogenization solution of the fine scale problem. Using homogenization theory, the Darcy relationship (2.5) can be rigorously derived from the fine scale equations (2.1) under the assumptions of scale separation and essential linearity. Consider a Navier–Stokes problem with scaling of the terms suitable for homogenization and numerical upscaling in porous media:

$$\begin{cases} \varepsilon^{\gamma}\vec{v}^{\varepsilon}\cdot\nabla\vec{v}^{\varepsilon}+\nabla p^{\varepsilon}-\varepsilon^{2}\mu\Delta\vec{v}^{\varepsilon}=\vec{f} & \text{in } \Omega^{\varepsilon},\\ \nabla\cdot\vec{v}^{\varepsilon}=0 & \text{in } \Omega^{\varepsilon},\\ \vec{v}^{\varepsilon}=0 & \text{on } \partial\Omega^{\varepsilon}, \end{cases} \tag{2.6}$$

where Ω^{ε} is the coarse domain Ω without the solid part. The parameter γ determines the strength of nonlinearity, smaller γ corresponds to larger nonlinearity. So, for $\gamma=\infty$ the equation is reduced to Stokes equation.

In [7, Thm. 1.1, p. 46; Thm. 2.4, p. 59; Thm. 2.5, p. 60] the following theorems are proved.

THEOREM 2.1. *For $\gamma>1$ and $\varepsilon\to 0$ there exists a homogenized solution for* (2.6)

$$\begin{cases} \vec{v}=\dfrac{1}{\mu}K\left(\vec{f}-\nabla p\right) & \text{in } \Omega,\\ \nabla\cdot\vec{v}=0 & \text{in } \Omega,\\ \vec{v}\cdot\vec{n}=0 & \text{on } \partial\Omega, \end{cases} \tag{2.7a}$$

$$K_{ij}=\int_{\beta}\nabla\vec{u}_i\cdot\nabla\vec{u}_j dy, \tag{2.7b}$$

$$\begin{cases} \nabla\pi_i-\Delta\vec{u}_i=\vec{e}_i & \text{in } \beta,\\ \nabla\cdot\vec{u}_i=0 & \text{in } \beta,\\ \vec{u}_i=0 & \text{in } \bar{\sigma},\\ \pi_i,\vec{u}_i, & y\text{-periodic}, \end{cases} \tag{2.7c}$$

where β is the porous part of the unit square domain where the fluid can flow, and σ is solid. $\beta\cup\bar{\sigma}$ forms the periodic unit cell scaled to a unit square; see Figure 1. *Scaling introduced in* (2.6) *results in K in* (2.7) *being the nondimentional permeability (see, e.g.,* [34]*).*

THEOREM 2.2. *For $\gamma=1$ and $\varepsilon\to 0$ there exists a homogenized solution for* (2.6)*:*

$$\nabla_y p_1+\vec{v}_0\cdot\nabla_y v_0-\mu\nabla_y^2\vec{v}_0=\vec{f}(\vec{x})-\nabla p(\vec{x}) \qquad \text{in } \beta\times\Omega, \tag{2.8a}$$

$$\nabla_y\cdot\vec{v}_0=0 \qquad \text{in } \beta\times\Omega, \tag{2.8b}$$

$$\nabla_x\cdot\vec{v}=0 \qquad \text{in } \Omega, \tag{2.8c}$$

$$\vec{v}\cdot\vec{n}=0 \qquad \text{on } \partial\Omega, \tag{2.8d}$$

$$\vec{v}_0,p_1, \qquad y\text{-periodic}, \tag{2.8e}$$

$$\vec{v}=\int_{\beta}\vec{v}_0 dy, \tag{2.8f}$$

where notation from Theorem 2.1 *is used; in addition, y represents the fast periodic variable and $\vec{v}_0$ and p_1 are auxiliary variables that for this truly nonlinear case cannot be decoupled.*

In the next section we will introduce a numerical method that can handle cases without separation of scales and nonperiodic media. The above theorems will serve as a useful benchmark for this numerical scheme when the corresponding assumptions are satisfied.

3. Method description. In this section we describe a method to compute the flux expression (2.4) by using multiscale techniques. The method is formulated in the framework of the HMM [19] to which we first give a brief introduction.

3.1. The HMM. An HMM for a two scale problem considers two sets of equations:

- coarse scale: $F(\boldsymbol{U}, \boldsymbol{D}) = 0$;
- fine scale: $f(\boldsymbol{u}, b) = 0$.

Here $\boldsymbol{U}$ and $\boldsymbol{u}$ are the functions that we are seeking the solution for, while $\boldsymbol{D}$ and b are data. Unknown quantities are marked as bold and, crucially, the coarse scale equation contains unknown data $\boldsymbol{D}$. In the HMM framework the aim is to solve the coarse equation, and to obtain necessary information on $\boldsymbol{D}$ by solving localized fine scale problems. Thus together with the equations one should specify operators to transfer information between the two scales. This involves both constraints to formulate local fine scale problems based on the coarse state and data estimation to recover coarse scale data from the solution of the fine scale problem.

3.2. The HMM for flow in porous media. To apply HMM to the problem outlined in section 2, discretization must be specified on both the coarse and the fine scale, as well as transfer operators between the scales.

3.2.1. Coarse scale discretization. To preserve conservation of mass the coarse continuity equation is discretized by a control volume method. For convenience of proofs in this paper we choose a control volume finite element formulation, although the methodology can be applied to more general control volume methods. Thus the coarse problem can be formulated as the following.

PROBLEM 3.1. *Consider a problem on a coarse domain Ω. Find p, such that for all Lipschitz subdomains $\tau \subset \Omega$*

$$\int_{\partial\tau} \vec{F}(\nabla p, \vec{x}) \cdot \vec{n} ds = \int_{\tau} f dx, \tag{3.1}$$

where $\vec{n}$ is the outward pointing normal and f is the function that represents the volumetric source density inside τ.

The operator $\vec{F}$ in terms of HMM is the data estimation operator.

To proceed to a numerical method we introduce a triangulation (with no loss of generality we describe the two-dimensional (2D) version of the algorithm); see Figure 2. The pressure is represented by a linear function on each triangle, and it can thus be represented by its value in the vertexes. The control volume grid is the Voronoi diagram that is dual to the triangulation (marked by red on Figure 2). We require that (3.1) is satisfied for all triangles in the grid (replacing τ). However instead of computing $\vec{F}(\nabla p, \vec{x})$ purely on the coarse scale by introducing, e.g., a Darcy relationship between the flux and the pressure gradient, the flux is estimated by solving a fine scale problem around a quadrature point on an edge of the triangle. To define this fine scale problem, we must first define a projection of the coarse pressure onto the fine scale.

3.2.2. Transfer from coarse to fine scale problem. Since the coarse scale flux is driven by pressure differences, as indicated by the functional form $\vec{F}(\nabla p, \vec{x})$, the fine scale problem should be formulated to account for this pressure difference. A natural way of projecting the coarse pressure difference onto the fine scale is to adjust the fine scale boundary conditions. Consider a local crop of the coarse scale grid as

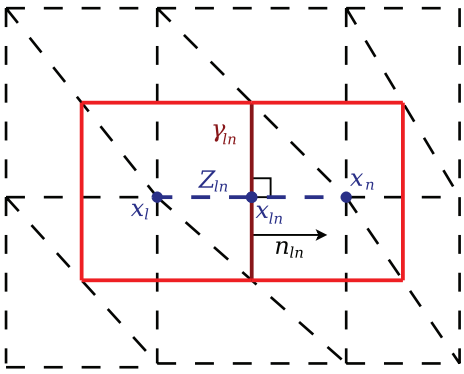

FIG. 2. *The structure of finite element grid (dashed lines) and the Voronoi finite volume grid dual to it (solid lines).*

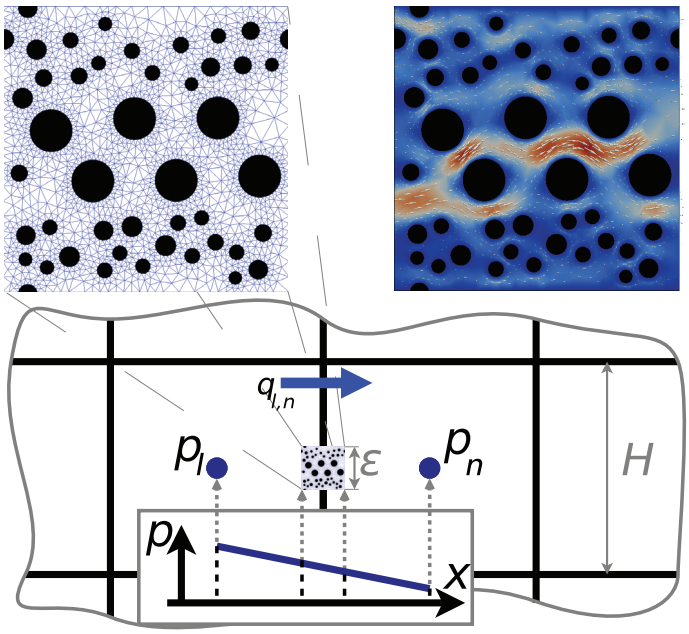

FIG. 3. *Building blocks of the multiscale method from the coarse grid perspective, zoom in to fine scale grid, and an example of flow solution on the fine grid.*

shown on Figure 2. We will describe how to set up the fine scale problem to estimate the flux between $\vec{x}_l$ and $\vec{x}_n$. By assumption 2 in section 4.1, as our grid is aligned with the axes, flow over a coarse edge will only be driven by the pressure difference between the two adjacent cells. Therefore the fine scale boundary conditions can be defined based on only p_l and p_n. To form boundary conditions for a local problem of the type (2.1) we project pressure to the fine scale problem defined on $\beta(\vec{x}_{ln})$ as it is shown on Figure 3:

$$p(\vec{x}) = \tilde{p}_l, \qquad \vec{x} \in \partial\beta_l, \tag{3.2}$$

$$p(\vec{x}) = \tilde{p}_n, \qquad \vec{x} \in \partial\beta_n, \tag{3.3}$$

where $\tilde{p}_l$ and $\tilde{p}_n$ are linear projections of p_l and p_n on the domain boundary as shown on Figure 3; β is the fine cell (see Definition 4.2); $\partial\beta_\xi$ ($\xi \in l, n, t, b$) are the corresponding parts of the external boundary of a fine cell; see Figure 1(c).

3.2.3. Fine scale discretization. The pressure projection described above defines some of the boundary conditions needed to solve the fine scale Stokes problem. For desirable cases where we can identify a periodic cell, for the top and bottom boundary the pressure is set to be periodic.[1] Moreover, the velocity is set as periodic on both the top-bottom and the left-right boundaries. On the internal boundaries, no-flow conditions are assigned. As it is shown later those boundary conditions are consistent with homogenization results.

Since the typical time scale of a fine scale cell problem is much smaller than one of the coarse scale it is fair to assume that in (2.1b) $\frac{\partial \vec{v}^\epsilon}{\partial t} = \vec{0}$. Taking into account this assumption the fine scale problem can be summarized as follows.

PROBLEM 3.2. *The fine scale cell problem takes the following form:*

$$[\vec{v} \cdot \nabla \vec{v}] + \nabla p - \mu \Delta \vec{v} = 0, \tag{3.4a}$$

$$\nabla \cdot \vec{v} = 0, \tag{3.4b}$$

with the boundary conditions

$$p(\vec{x}) = \tilde{p}_l, \qquad \vec{x} \in \partial\beta_l, \tag{3.4c}$$

$$p(\vec{x}) = \tilde{p}_n, \qquad \vec{x} \in \partial\beta_n, \tag{3.4d}$$

$$\vec{v}(\vec{x}) = \vec{0}, \qquad \vec{x} \in \bar{\sigma}, \tag{3.4e}$$

$$p, \vec{v} \text{—periodic on the square elsewhere,} \tag{3.4f}$$

following the notation from Figure 1(c). *Neglecting the term in the brackets in* (3.4a) *results in a linear problem that is analyzed in most of the paper.*

In our HMM we will solve Problem 3.2 numerically. To this end we introduce a triangulation as illustrated on Figure 1(c) and discretize the problem by Taylor–Hood elements using FEniCs [31]. The possibility of having different solvers on different scales is one of the key features of the HMM framework that is also utilized in the method described in our paper where mixed finite elements are used on the fine scale and control volumes are used for the coarse scale. For convenience the fine local problem is rescaled to a unit square domain β. This results in the full fine scale problem being scaled as (2.6).

Remark 3.3. The methodology described in this paper is not limited by the periodicity assumptions and can be applied on general representative elementary volumes with different boundary conditions, such as zero Dirichlet on top-bottom and Neumann on left-right. For the latter case on general geometries the proofs cannot be conducted and hence it is not described in more detail. The interested reader may find a discussion about effects of boundary conditions for similar upscaling problems in, e.g., [17].

3.2.4. Computation of coarse scale flux. The coarse flux density is computed by integrating the horizontal component of the velocity in the fine scale problem from top to bottom and dividing it by the cell size ε. Incompressibility of the fine scale

[1] For general geometry different possible boundary conditions are described in Remark 3.3.

problem allows us to perform this procedure in any cross section of the fine scale cell problem.

Remark 3.4. It is important to note that in practice, to save computational effort, one can perform computations in the call-by-need manner, meaning that for a given geometry we store previous computations and reuse these result in future. For the linear problem with periodic media this means that the total computational effort on the fine scale would be solving only one local problem, which is equivalent to the effort spent in traditional upscaling methods.

3.2.5. Summary of the algorithm. The algorithm to solve for the coarse scale pressure and fluxes can be summarized as follows.

1. Start with a guess of the coarse pressure in all cells.
2. Estimate the flux over the coarse edges from the pressure drop over the edge. If a flux for a similar pressure drop and grain structure is available from a previous calculation, use this. If not, invoke the fine scale solver.
3. Compute the residual from the new fluxes equal to the difference between sources and total outflow in each coarse cell. If this is sufficiently small, the solution is found. If not, update the coarse pressure by an iterative method based on the residual and go to point 1 (in our implementation for simplicity we use a Newton-type method that converges in a few iterations for flow regimes we have tested the method on).

3.3. Location of quadrature points. The method described in section 3.2 is a straightforward generalization of the control volume finite element method (CVFEM) to the HMM framework. The straightforward quadrature approximation introduced in the description of the method in section 3.2.2 can be formally expressed as

$$\vec{F}_q^{FE}(\vec{x}_{ln}, p_l, p_n) = \vec{F}\left(\frac{p_l - p_n}{|Z_{ln}|}, \vec{x}_{ln}\right) = \vec{F}\left(\nabla p_H(\vec{x}_{ln}), \vec{x}_{ln}\right), \tag{3.5}$$

where index q stands for quadrature approximation and FE indicates it mimics CVFEM behavior; $\frac{p_n - p_l}{|Z_{ln}|}$ is a finite element (FE) approximation to the gradient parallel component and p_H is a notation for the finite element approximation of the pressure.

However, for media with high permeability contrasts that are roughly resolved by the control volumes (see Figure 4), CVFEM gives a poor approximation of the pressure drop, and thus the flux. The reason is that a linear pressure interpolation between cell centers cannot capture the discontinuity in the pressure gradient associated with the jump in the permeability. Therefore, the flux computed by the CVFEM-based HMM method will be highly dependent on the location of the quadrature point; see Figure 4(a).

A control volume method commonly used to simulate porous media flow is the so-called two point flux approximation (TPFA) that is derived as a mass conservative finite difference method. In TPFA an auxiliary pressure is introduced at the interface between the control volumes, and using this TPFA will correctly compute an interface transmissivity equal to the harmonic mean. Thus for heterogeneous media, it is of interest to consider control volume HMM based on TPFA. To do so an auxiliary pressure variable is introduced at a point $\vec{x}_{ln}$ on the interface between two control volumes; see Figure 4(b). This splits the local problem between point $\vec{x}_l$ and $\vec{x}_n$ into two. We again assume pressure varies linearly between each two neighboring points and hence perform the same interpolation as in section 3.2 on both sides from $\vec{x}_{ln}$; see

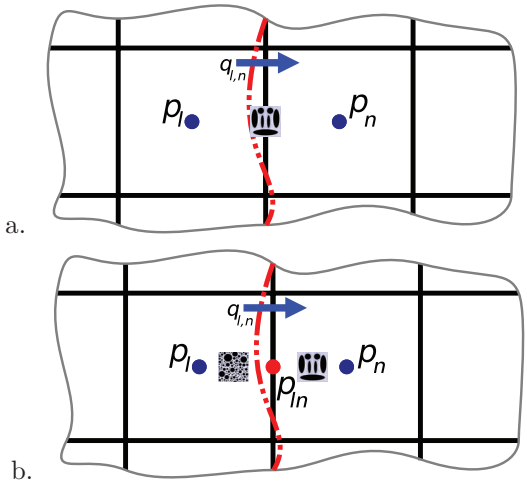

FIG. 4. *Handling of discontinuity roughly resolved by coarse grid by methods utilizing two types of quadrature approximation: CVFEM style* (a) *and TPFA style* (b).

Figure 3. After integrating the results from the auxiliary problems, p_{ln} is eliminated. As the problem is local the continuity equation implies that the flux between the two cells will be the same in all cross sections along Z_{ln}. This means that for the linear problem the permeability computed in such a way will be equal to the harmonic mean and hence this choice of quadrature will mimic the TPFA. This can be more formally written in a way similar to (3.5),

(3.6)
$$F_{q\|}^{TPFA}(\vec{x}_{ln}, p_l, p_n) = \left(\frac{|\vec{x}_{ln} - \vec{x}_l|}{|Z_{ln}|} \left[F_{\|} \left(\nabla p_H(\vec{x}_{ln}), \frac{\vec{x}_{ln} + \vec{x}_l}{2} \right) \right]^{-1} + \frac{|\vec{x}_{ln} - \vec{x}_n|}{|Z_{ln}|} \left[F_{\|} \left(\nabla p_H(\vec{x}_{ln}), \frac{\vec{x}_{ln} + \vec{x}_n}{2} \right) \right]^{-1} \right)^{-1},$$

where $\|$ indicates that this is a component parallel to the flow and the right-hand side is the harmonic mean.

The TPFA-based approximation also introduced earlier in [8] differs significantly from older publications that consider control volume multiscale methods and only use a one point approximation, such as [6]. The error introduced by using different quadrature approximations is estimated in Remark 5.12. The practical applicability of choices of quadrature points is considered in the numerical experiments in section 7.2.

4. Assumptions. In this paper we will limit ourselves to 2D problems. Moreover, in order to carry out proofs in this paper some assumptions to both the coarse and the fine problem should be introduced.

4.1. Fine scale assumptions.

1. On the fine scale it is assumed that porous geometry is known and periodic with period ε within large subdomains.
2. The pore structure is assumed to be aligned with the coarse grid, in the sense that flow normal to the coarse edges is only driven by the corresponding

normal component of the coarse pressure gradient. For Darcy's law this means that the permeability tensor K in (2.5) is diagonal in the coordinate system of the grid (for Cartesian grids).

3. Furthermore we introduce some simplifications to (2.1b):
   - There are no volumetric forces; $\vec{f} = \vec{0}$.
   - The velocities are small so that the nonlinear term $\vec{v}^\varepsilon \cdot \nabla \vec{v}^\varepsilon$ is negligible. In most of the paper we assume it is exactly zero.

Remark 4.1. The simplifications concerning (2.1b) introduced in assumption 3 will be used in proofs in section 5. Section 6, however will weaken them and present the sketches of the proofs for weakly nonlinear fine scale problem and discuss applicability of the framework to fully nonlinear flow.

4.2. Coarse scale assumptions. The convergence proof for the coarse pressure assumes that the solution p lies in the space

$$p \in \mathcal{H}_0^{(2)}(\Omega) \equiv \mathcal{H}_0^1(\Omega) \cap \mathcal{H}^2(\Omega), \tag{4.1}$$

where Ω is the coarse domain of the problem. According to Cai, Mandel, and McCormick [12] sufficient requirements on the problem to possess property (4.1) are

1. the components of permeability tensor K_{ii} are continuous;
2. the source term $f \in L_2(\Omega)$;
3. the domain Ω is convex.

Requirement 1 relies on the fine scale. In order to fulfill it we define the the flux function $F(\nabla p, \vec{x})$ described in (2.4) to be a solution to the fine scale problem on a square domain β^ε around $\vec{x}$ defined as

$$\beta^\varepsilon = \left[\vec{x}_1 - \frac{\varepsilon}{2}, \vec{x}_1 + \frac{\varepsilon}{2}\right] \times \left[\vec{x}_2 - \frac{\varepsilon}{2}, \vec{x}_2 + \frac{\varepsilon}{2}\right]. \tag{4.2}$$

Perturbations in $\vec{x}$ on a scale much smaller than ε will result in small perturbations of the local fine scale domain configuration and hence the solution, that for the linear case means continuous permeability.

Further on in the paper we will need a slightly different definition of local fine scale domain.

DEFINITION 4.2. *The fine cell domain β is the fluid part of β^ε defined by* (4.2) *scaled to the unit square.*

5. An a priori error estimate. In this subsection we will estimate the $\mathcal{H}^1$ norm of the difference in pressure between the HMM solution and the real solution. We start by explaining the error contributors and later prove the estimate for each of them separately.

By repeated application of the triangle inequality, the difference between the true averaged solution p and the fully discrete coarse solution obtained from HMM, $p_{MS}^{H,h}$, can be expressed as in [5],

$$\left\| p_0 - p_{MS}^{H,h} \right\|_{\mathcal{H}^1} \leq \left\| p_0 - p_{MS}^{0,0} \right\|_{\mathcal{H}^1} \tag{5.1}$$

$$+ \left\| p_{MS}^{0,0} - p_{MS}^{0,h} \right\|_{\mathcal{H}^1} \tag{5.2}$$

$$+ \left\| p_{MS}^{0,h} - p_{MS}^{H,h} \right\|_{\mathcal{H}^1} \tag{5.3}$$

$$\leq C \left(\eta + \left(\frac{h}{\varepsilon} \right)^\alpha + H \right). \tag{5.4}$$

The auxiliary terms in (5.1)–(5.3) have the following meaning:

- p_0: The exact solution of the homogenized problem when $\varepsilon \to 0$;
- $p_{MS}^{0,0}$: The solution by the multiscale method when both scales are solved exactly;
- $p_{MS}^{0,h}$: The solution by the multiscale method when the coarse scale is solved exactly, but the fine scale is solved on the h-size grid;
- $p_{MS}^{H,h}$: The solution by the fully discrete multiscale method (with H and h grids).

With this in mind we identify the terms in (5.1)–(5.3) in the following way.

(5.1) *Modeling error.* The error from substituting the correct cell problem with an approximate one.

(5.2) *Propagation of fine scale error.* The error due to solving cell problem numerically on a grid with cell sizes h/ε.

(5.3) *Coarse scale error.* The error due to solving the coarse problem numerically on a grid with cell size H and using quadrature approximation for the flux term.

Remark 5.1 (nonlinear modeling error $C\eta$). In (5.4) the modeling error (5.1) is estimated to be proportional to η which is a measure of nonlinearity, that is a more general statement than is proven in this section. In this section the fine scale problem is assumed to be linear and hence $\eta = 0$. This is proven in Theorem 5.6.

For a weakly nonlinear flow, η describes the deviation of the flux from linear (6.1). More general estimates, for the case when $\eta > 0$, are discussed in section 6.1.

Remark 5.2 (different ways of treating the propagation of fine scale error). In most previous works, in which analysis of HMMs is carried out (e.g., [4, 5]), the splitting into error terms was done differently. Namely, in the chain of triangle inequalities the fine scale discretization error was introduced after the coarse scale error. In the analysis phase this leads to analyzing $\|p_{MS}^{H,0} - p_{MS}^{H,h}\|_{\mathcal{H}^1}$ rather than $\|p_{MS}^{0,0} - p_{MS}^{0,h}\|_{\mathcal{H}^1}$ in our case. While both approaches are valid the one used in this paper allows proofs to be carried out in a continuous setting that can be more convenient, for example, for nonlinearly driven problems.

Equation (5.4) is the summary of the error terms following the estimates formulated in the rest of the section as theorems.

5.1. Modeling error. In this subsection we prove that for linear problem on the fine scale, our HMM represents a method of numerical upscaling consistent with homogenization solutions. The proof is split into several lemmas and it is summarized in Theorem 5.6.

5.1.1. Equivalence on the fine scale. We start by proving the equivalence of cell problem formulations in our multiscale method and in homogenization

LEMMA 5.3. *The velocity solution $\vec{u}$ of the homogenization cell problem given by* (2.7c) *is equivalent to the solution of the fine scale problem in the HMM* (3.4) *with the following scaling*

$$\vec{u}_i = \frac{\mu}{\delta p_1} \vec{v}_i, \tag{5.5}$$

where δp_1 is defined as pressure drop between the boundary conditions (3.4c), (3.4d) $\delta p_1 = \tilde{p}_n - \tilde{p}_l$.

Proof. The weak formulation of (2.7c) can be written in a weak form [33, Chapter 9].

PROBLEM 5.4. *Find* $\vec{u} \in \mathcal{H}^1_{per,div0}$ *such that for all* $\vec{w} \in \mathcal{H}^1_{per,div0}$

$$\int_\beta \nabla \vec{u}_i : \nabla \vec{w} = \int_\beta \vec{f} \cdot \vec{w}, \tag{5.6}$$

where for the considered case the force $\vec{f} = \vec{e}_i$*. Index* $div0$ *means that it is a subspace of divergence free functions.*

The formulation (5.6) gives the unique solution for velocity $\vec{u}_i$ for (2.7c). The absence of pressure in (5.6) implies that the pressure is an auxiliary variable in the Stokes equations and does not influence $\vec{u}_i$.

If $\vec{f} = \nabla\psi$ is a potential vector field then (5.6) can be further rewritten, using the properties of $\vec{w}$,

$$\int_\beta \nabla \vec{u}_i : \nabla \vec{w} = \int_\beta \nabla\psi \cdot \vec{w} = \int_{\partial\beta} \psi \vec{n} \cdot \vec{w} - \int_\beta \psi \nabla \cdot \vec{w} = \int_{\partial\beta} \psi \vec{n} \cdot \vec{w}, \tag{5.7}$$

that also implies that ψ can be replaced by any other function that has the same values on the boundary.

A potential corresponding to the force in our case is $\psi = x_i + c$, where x_i is the ith coordinate and c is an arbitrary constant. To achieve our goal we choose c such that $\psi = \tilde{p}_l/\delta p_1$ on $\partial\beta_l$ implying the right boundary condition $\psi = \tilde{p}_l/\delta p_1 + 1$ on ∂D_l. The boundary conditions on the remaining sides of the domain can be set to $\psi = x_i + c$ or even simply forced to be periodic since it will not change the behavior of the right-hand side integral in (5.7).

After those modifications the differences between HMM fine scale problem and homogenization cell problem are the viscosity factor μ in front of $\vec{v}^\varepsilon$ and the factor in the boundary conditions δp_1. Due to linearity the two solutions are equivalent with the scaling given by (5.5). ∎

5.1.2. Equivalence in data estimation. Second, we should prove that for the linear case the data estimation operator $\vec{F}(\vec{x}, \nabla p)$ is equivalent to the averaging done in homogenization to compute the flux density in (2.7a) and (2.7b). By the assumptions in section 4.1 the flow is driven only by a difference in the pressure and hence in (2.7a) $\vec{f} = 0$.

We start by proving an auxiliary lemma interpreting equation (2.7b).

LEMMA 5.5. *The integration in* (2.7b) *to compute* K_{ii} *is equivalent to integration of the* i*th velocity component across the cell perpendicular to* $\vec{e}_i$*,*

$$K_{ii} = \int_\beta \nabla \vec{u}_i : \nabla \vec{u}_i dx = \int_{\beta_i(x_i)} \vec{u}_i \cdot \vec{n}_i ds, \tag{5.8}$$

where $\beta_i(x_i)$ *is a plane perpendicular to* $\vec{e}_i$ *at point with coordinate* x_i*.*

Proof. Choosing the test function in Problem (5.4) as $\vec{u}_i$ gives a simplified expression for K_{ii},

$$K_{ii} = \int_\beta \nabla \vec{u}_i : \nabla \vec{u}_i dx = \int_\beta \vec{e}_i \cdot \vec{u}_i dx. \tag{5.9}$$

Periodic boundary conditions provide mass conservation along e_i meaning that the integral flux in the direction of e_i over each perpendicular cross section is constant

with respect to the normal spatial direction. Thus

$$\int_\beta \vec{e}_i \cdot \vec{u}_i dx = \int_0^1 \int_{\beta_i(x_i^0)} \vec{u}_i(x_i) \cdot \vec{n}_i ds dx_i$$
$$= \int_0^1 1 dx_i \int_{\beta_i(x_i)} \vec{u}_i(x_i) \cdot \vec{n}_i ds = \int_{\beta_i(x_i)} \vec{u}_i(x_i) \cdot \vec{n}_i ds$$

that is by (5.9) the coefficient K_{ii}, concluding the lemma. □

The equivalence in data estimation is summarized in the following theorem.

THEOREM 5.6. *The homogenized solution is equivalent to the HMM problem when both the fine scale problem and the coarse scale problem are solved exactly and hence*

$$\left\| p^0 - p^{0,0}_{MS} \right\|_{\mathcal{H}^1} = 0. \tag{5.10}$$

Proof. To show the equivalence let us compare the data estimation expressions obtained by the HMM and homogenization.

The expression for the parallel component of the flux density $\vec{v}$ in the HMM as it is described in section 3.2.4 takes the form

$$\vec{v}_i^{HMM} = \frac{1}{\varepsilon} \int_{\beta_i} \vec{v}_i^\varepsilon \cdot \vec{n}_i = \frac{\delta p_1}{\mu\varepsilon} \int_{\beta_i} \vec{u}_i \cdot \vec{n}_i = -\frac{\varepsilon}{\mu\varepsilon} \frac{\partial p}{\partial x_i} \int_{\beta_i} \vec{u}_i \cdot \vec{n}_i$$
$$= -\frac{K_{ii}}{\mu} \frac{\partial p}{\partial x_i} - \frac{K_{ij}}{\mu} \frac{\partial p}{\partial x_j} = \vec{v}_i^{Hom}. \tag{5.11}$$

To carry out the chain of inequalities to achieve (5.11) we have used (5.5) from Lemma 5.3, the definition from (3.4d), the assumption that permeability is aligned with the grid, and the homogenized equation (2.7a).

The equality in (5.11) implies that for the linear case the HMM solved exactly coincides with the homogenization solution, meaning that the solutions are also the same and hence proving (5.10). □

5.2. Propagation of the fine scale error. The fine scale error (5.2) in our approximation is the combination of two multiplicative parts:

- the actual error induced by the approximate solution of the fine scale equations by a numerical method;
- the propagation of this error to the coarse solution.

We will consider here these two building blocks.

5.2.1. Fine scale error from finite element solution of the Stokes problem. The analysis of Taylor–Hood elements (see [24, Chapter II, 4.2] or [35]) gives the following estimate of the fine scale error,

$$\|\vec{v}_{i0}^\varepsilon - \vec{v}_{ih}^\varepsilon\|_{L^2(\beta)} \leq C_i \left(\frac{h}{\varepsilon}\right)^\alpha, \tag{5.12}$$

where $\vec{v}_{i0}^\varepsilon$ is exact solution to the Stokes problem and $\vec{v}_{ih}^\varepsilon$ is a numerical solution with Taylor–Hood elements on a grid with size h/ε. We note that the size h/ε is relative to the coarse grid, in the actual simulation the cell problem is scaled to the unit square and, hence, the estimate is of order h instead.

In (5.12) α depends on the fine cell geometry, i.e., the largest internal angles $1 \leq \alpha \leq 2$, where $\alpha = 2$ on convex domains and decreases with increase of internal angles over π [35]. For the cases of interest in this paper, where the grains are assumed to be polygons which are close to discs and hence have angles $\varphi \gtrapprox \pi$, the parameter α is close to 2.

5.2.2. Propagation of the fine scale error. The approximation of the fine scale velocity from (5.12) is integrated as it is described in section 5.1 to form the parameter field of the coarse scale problem. From (5.12) together with (5.9) and the Sobolev embedding theorem it follows that at each point in space

$$|K_{ii} - K_{ii}^h| \leq \left| \vec{e}_i \cdot \int_\beta (\vec{v}_{i0}^\varepsilon - \vec{v}_{ih}^\varepsilon)\, dx \right| \leq \|\vec{v}_{i0}^\varepsilon - \vec{v}_{ih}^\varepsilon\|_{L_1(\beta)} \leq C_i \left(\frac{h}{\varepsilon}\right)^\alpha.$$

Taking the 2-norm of the matrix K we end up with

$$\max_\Omega \|K - K^h\|_2 \leq C \left(\frac{h}{\varepsilon}\right)^\alpha. \tag{5.13}$$

Prior to proving the theorem providing the estimate let us introduce an important lemma that shows how the perturbation in data influences the error in the solution to an elliptic PDE in the weak form. Up till now we have been using a formulation of the PDE in the integral conservation form (Problem 3.1). However, for simplicity of proofs, it is more convenient to use the weak formulation of our problem, since the two formulations are equivalent when $f \in L^2$.

LEMMA 5.7. *Consider a PDE in the weak form*

$$a_\kappa(p, v) \equiv \int_\Omega \kappa \nabla p \cdot \nabla v dx = \int_\Omega f v dx. \tag{5.14}$$

Given two continuous parameter sets for the problem $\kappa = A$ and $\kappa = \tilde{A}$, such that both lead to an elliptic problem with the ellipticity constant γ,

$$a_\kappa(v, v) \geq \gamma \|v\|^2_{\mathcal{H}^1(\Omega)}. \tag{5.15}$$

If these parameter sets further satisfy

$$\max_\Omega \|A - \tilde{A}\|_2 \leq \lambda \tag{5.16}$$

then the corresponding solutions p and $\tilde{p}$ can be bounded in the sense

$$\|p - \tilde{p}\|_{\mathcal{H}^1} \leq C\lambda \|\nabla \tilde{p}\|_{L_2}, \tag{5.17}$$

where C is independent of A and $\tilde{A}$.

The proof of the lemma follows from [21, Lemma 1.8] The result of the lemma can be interpreted as the following.

COROLLARY 5.8. *If two problems of the form* (5.14) *with the restrictions* (5.15) *have solutions bounded in $\mathcal{H}^1$ norm*

$$p, \tilde{p} \in \mathcal{H}^1 \tag{5.18}$$

and the parameter fields are lying close in the sense of (5.16)*, then the solutions of those problems are close in the $\mathcal{H}^1$ norm*

$$\|p - \tilde{p}\|_{\mathcal{H}^1} \leq C\lambda. \tag{5.19}$$

Proof. The result follows from Lemma 5.7 by using the boundedness assumption (5.17). ∎

The following theorem gives the error estimate due to propagation of the fine scale error to the coarse scale.

THEOREM 5.9. *The propagation of the fine scale error onto the coarse scale is bounded as*

$$\left\| p_{MS}^{0,0} - p_{MS}^{0,h} \right\|_{\mathcal{H}^1} \leq C \left(\frac{h}{\varepsilon} \right)^{\alpha}. \tag{5.20}$$

Proof. Since both $p_{MS}^{0,0}$ and $p_{MS}^{0,0}$ are solutions to continuous problems the proof can be carried out in the set up of the weak formulation. Moreover the solutions are in $\mathcal{H}^1$ by assumptions of the paper (see section 4.2). Applying Corollary 5.8 with $\lambda = C(\frac{h}{\varepsilon})^{\alpha}$ gives the result of the theorem. ∎

5.3. Coarse scale error from finite volume approximation. In order to prove the estimate on the coarse scale we will follow the proof in [12], and introduce the quadrature approximation whenever needed. For convenience of notation let us omit unused indexes

$$p_{MS}^{\xi,h} \equiv p^{\xi}; \tag{5.21}$$

let us also introduce the notation for the equation coefficient to replace the fraction

$$A^{\xi} = \frac{K^{\xi}}{\mu}. \tag{5.22}$$

Since the flow is assumed to be linear, the flux achieved from the fine scale computation will correspond to the Darcy relation (2.5) with an appropriate permeability field as is shown in section 5.1, and the solution approaches of the method on the two scales decouples. Moreover, this permeability and hence the parameter field A are essentially smooth.

The CVFEM is defined as follows [12].

PROBLEM 5.10. *Find $\tilde{p}^H \in S_0^H$ (the space of piecewise-linear finite elements), such that for all grid cells τ^H the equality below is satisfied:*

$$-\int_{\partial \tau^H} (A \nabla \tilde{p}^H) \cdot \vec{n} ds = \int_{\tau^H} f dx, \tag{5.23}$$

where A is a continuous parameter field on the coarse scale. In other words, $\tilde{p}^H$ is a finite element solution to the problem where no quadrature is introduced.

Let us also define a linear operator $B : S_0^H + \mathcal{H}_0^{(2)} \to \mathcal{R}^n$ associated with the left-hand side of the equation above:

$$b_{ln}(v) = -\int_{\gamma_{ln}} (A \nabla v) \cdot \vec{n}_{ln} ds, \tag{5.24}$$

$$Bv = \left(\sum_{n \in \omega_l} b_{ln} v \right)_{l \in I} = \left(-\int_{\partial \tau_l} (A \nabla v) \cdot \vec{n} ds \right)_{l \in I}, \tag{5.25}$$

where γ_{ln} is the boundary between control volumes around l and n (see Figure 2), ω_l is the set of vertices adjacent to l, and I is the index set for all vertices in the finite element space. We will also consider the continuous problem analogous to Problem 3.1,

$$-\int_{\partial V} (A \nabla p^0) \cdot \vec{n} ds = \int_V f dx, \tag{5.26}$$

where V is any Lipshitz subdomain of Ω.

Finally, we will consider the discrete problem

$$-\int_{\partial\tau^H}(A^H\nabla p^H)\cdot\vec{n}ds=\int_{\tau^H}fdx, \tag{5.27}$$

where A^H is chosen, such that the quadrature rule is satisfied,

$$F_{q\|}(\nabla q^H)\big|_{ln}=\int_{\gamma_{ln}}(A^H\nabla q^H)\cdot\vec{n}ds, \tag{5.28}$$

where $F_{q\|}(\nabla q^H)$ is the discrete approximation to the flux function made by our multiscale method and $q^H\in S_0^H$. We choose A^H to be a sufficiently smooth function that satisfies (5.28). If we want it to be continuous it can be chosen from the second order polynomials on the edges and interpolated appropriately inside the domain.

LEMMA 5.11. *There exists an A^H sufficiently smooth and strictly positive definite such that* (5.28) *is satisfied, which is sufficiently close to the given A*

$$\max_{x\in\Omega}\left\|A^H-A\right\|_2\le CH. \tag{5.29}$$

Proof. We give an algorithm to construct such an A^H. First let us define a quadrature value of A on every edge that we denote by A_q,

$$|\gamma_{ln}|\vec{n}_{ln}\cdot A_q^{ln}\vec{e}_k=\vec{F}_{q\|}(\vec{e}_k)\Big|_{ln}, \tag{5.30}$$

where unit vector $\vec{e}_k$ replaces the pressure gradient and superscript ln indicates the edge between control volume l and n in the grid. From here we follow three steps to construct A^H on entities of the grid.

1. On the vertices of the control volume grid we set
$$A^H(x)=\min_{\forall i_1i_2,x\in\gamma_{i_1i_2}}\left(A_q^{i_1i_2}\right).$$
2. On the edges of the control volume grid A^H is approximated by a polynomial that satisfies step 1 and respects the quadrature rule (5.28) in terms of (5.30),
$$\int_{\gamma_{ln}}\vec{n}\cdot A^H\vec{e}_kds=|\gamma_{ln}|\vec{n}_{ln}\cdot A_q\vec{e}_k=\vec{F}_{q\|}(\vec{e}_k)\Big|_{ln}. \tag{5.31}$$
3. Elsewhere A^H is interpolated smoothly, e.g., by a harmonic function respecting steps 1 and 2.

The minima of A^H defined by the steps above are guaranteed to be located in the vertices of the control volume grid and the positive definiteness of KH is guaranteed by positive definiteness of A_q that follows from properties of fine scale.

Due to continuity, the derivative is bounded and hence A^H approximates A_q that is extended to a piecewise constant around quadrature points as

$$\max\left\|A_q-A^H\right\|_2\le CH \tag{5.32}$$

by construction. For the quadrature choices of this paper, a piecewise constant approximation of A_q also gives $\max\|A-A_q\|_2\le CH$ (see Remark 5.12 below), hence proving the lemma. ∎

Remark 5.12 (specific choices of quadrature rules). If the permeability function A is in W_∞^1 or, in other words, has its derivative's variation limited in the weak sense then for a finite volume approximation given by (3.5) we have

$$\left\|A-A_q^{FE}\right\|_2\le CH, \tag{5.33}$$

since A_q along the edge is equal to its value in the midpoint.

For the case of TPFA for which it is expressed in terms of the harmonic mean (3.6) the result is obtained by use of the triangle inequality once more. In the worst scenario

(5.34)
$$\left\|A - A_q^{TPFA}\right\|_2 \leq CH + \max(\|A(\vec{x}_{ln}) - A(\vec{x}_l)\|_2, \|A(\vec{x}_{ln}) - A(\vec{x}_n)\|_2) \leq 2CH.$$

The latter result (5.34) gives the same asymptotic rate as (5.33), but has a worse constant. It should be noted that in applications, the assumption on continuity of the permeability is too strong; in practice material discontinuities that are approximately resolved by the coarse grid are as common. In such cases the TPFA quadrature produces more accurate results as illustrated by a numerical example in section 7.2.

With results for the quadrature approximation at hand we can proceed to estimating the norm of the coarse scale error. We construct finite elements for our CVFEM as triangles with degrees of freedom corresponding to potential lying on the mesh corners as was discussed in section 3.2.1. For the case when the control volumes are rectangles the triangles would be right angled and there will be no flow along the hypotenuse due to orthogonality (the length of the dual grid's side is equal to 0; see Figure 2).

We want to estimate the error in the discrete seminorm

$$|p|_{1,\bar{\Omega}^H} = \sqrt{\sum_{l,n} (p(x_l) - p(x_n))^2 \frac{|\gamma_{ln}|}{|Z_{ln}|}}, \tag{5.35}$$

where γ_{ln} and Z_{ln} are illustrated on Figure 2.

The goal is to achieve a bound for the error between the correct solution of the problem p^0 and the CVFE solution on the H-sized grid using quadrature integration p^H. Using the triangle inequality a norm of the error can be split,

$$\left\|p^0 - p^H\right\|_{\mathcal{H}^1} \leq \left\|p^0 - \tilde{p}^H\right\|_{\mathcal{H}^1} + \left\|\tilde{p}^H - p^H\right\|_{\mathcal{H}^1}, \tag{5.36}$$

where $\left\|p^0 - \tilde{p}^H\right\|_{\mathcal{H}^1}$ is the error due to the finite element approximation and $\left\|\tilde{p}^H - p^H\right\|_{\mathcal{H}^1}$ is the error due to the quadrature approximation of A by A^H. In the paper by Cai, Mandel, and McCormick [12] the estimate for the first term is given in the sense of the seminorm from (5.35) in Theorem 1 from [12]:

$$\left|p^0 - \tilde{p}^H\right|_{1,\bar{\Omega}^H} \leq CH. \tag{5.37}$$

We need to estimate the second term $|\tilde{p}^H - p^H|_{1,\bar{\Omega}^H}$. The estimate is proved in the following lemma.

LEMMA 5.13. *The seminorm due to quadrature approximation on the coarse scale is limited by the coarse grid resolution H,*

$$|e^q|_{1,\bar{\Omega}^H} \equiv \left|\tilde{p}^H - p^H\right|_{1,\bar{\Omega}^H} \leq CH. \tag{5.38}$$

Proof. In [12] it is proved that under our assumptions on the permeability tensor (orientation along the grid and continuity/smoothness) the operator B is uniformly elliptic on our finite element function space S_0^H; see Lemma 2 in [12], or formally

$$\sum_{l \in I} v(x_l)(Bv)_l \geq \gamma |v|^2_{1,\tilde{\Omega}^H} \tag{5.39}$$

for all v in S_0^H. Let us use this inequality to do the following estimate,

$$\gamma \left|\tilde{p}^H - p^H\right|^2_{1,\bar{\Omega}^H} \leq \sum_{l\in I} e^q(x_l)(Be^q)_l \tag{5.40}$$

$$= -\sum_{l\in I} e^q(x_l) \int_{\partial\tau_l} (A\nabla\tilde{p}^H - A\nabla p^H)\cdot\vec{n}_l ds$$

$$= -\sum_{l\in I} e^q(x_l) \left(\int_{\partial\tau_l} ((A^H - A)\nabla p^H)\cdot\vec{n}_l ds\right), \tag{5.41}$$

where we have combined (5.23) and (5.27) for all control volumes in the grid. By the properties of quadrature derived in Lemma 5.11 we have a bound of the form (5.29) for the difference between the correct and approximate permeability. Using the inequality (5.29) and the Cauchy–Schwarz inequality leads to

$$\begin{aligned}
&-\sum_{l\in I} e^q(x_l) \left(\int_{\partial\tau_l} ((A^H - A)\nabla p^H)\cdot\vec{n}_l ds\right)\\
&\leq -CH\sum_{l\in I} e^q(x_l)\int_{\partial\tau_l} (\nabla p^H)\cdot\vec{n}_l ds\\
&= CH\sum_{l\in I} e^q(x_l)\sum_{n\in\omega_l}\int_{\gamma_{ln}} (\nabla p^H)\cdot\vec{n}_l ds\\
&= CH\sum_{\{l,n\}\in\omega} (e^q(x_n) - e^q(x_l))\int_{\gamma_{ln}} (\nabla p^H)\cdot\vec{n}_l ds\\
&\leq CH\left|e^q\right|_{1,\bar{\Omega}^H}\left(\sum_{\{l,n\}\in\omega}\left(\int_{\gamma_{ln}} (\nabla p^H)\cdot\vec{n}_l ds\right)^2 \frac{|Z_{ln}|}{|\gamma_{ln}|}\right)^{\frac{1}{2}}.
\end{aligned}$$

Division by $|e^q|$ results in the inequality

$$\left|e^q\right|_{1,\bar{\Omega}^H} \leq CH\left[\sum_{\{l,n\}\in\omega}\left(\int_{\gamma_{ln}} (\nabla p^H)\cdot\vec{n}_l ds\right)^2 \frac{|Z_{ln}|}{|\gamma_{ln}|}\right]^{\frac{1}{2}}. \tag{5.42}$$

We need to ensure that the expression in the brackets in (5.42) is bounded. Since the properties of A^H from Lemma 5.11 are no worse than the properties of the original A we can formulate a continuous problem similar to (3.1) replacing A by A^H in the data estimation function

$$-\int_{\partial\tau} (A^H\nabla\sigma^H)\cdot\vec{n} ds = \int_\tau f dx, \tag{5.43}$$

and σ^H will be the unique solution to the problem. Moreover functions $p^H_{\delta x}$ (for which data estimation is fixed to H but the grid is further refined to δx and $p^H_H \equiv p^H$ by our definition) will converge to this solution σ^H with refinement of δx,

$$p^H_{\delta x} \to \sigma^H \text{ as } \delta x \to 0 \tag{5.44}$$

as proven in [12, Theorem 1].

The exact solution to the approximate problem, σ^H, lies in the same space as p^H as its parameter field is no worse, meaning that it converges to p with refinements as A^H goes to A by Lemma 5.7:

$$\sigma^H \to p. \tag{5.45}$$

From (5.44) and (5.45) we conclude that p^H converges to p which means that it is also bounded in $\mathcal{H}^1$ norm; and hence the right-hand side in (5.42) is bounded by CH, proving (5.38). ∎

COROLLARY 5.14. *The full coarse error is limited in the seminorm,*

$$|e^c|_{1,\bar{\Omega}^H} \equiv \left|p^0 - p^H\right|_{1,\bar{\Omega}^H} \leq CH. \tag{5.46}$$

Proof. The result follows directly from the theorem above and Theorem 1 from [12]. ∎

To bring the results back to the norms we started out with, i.e., $\mathcal{H}^1$, we first use interpolation from finite element space of piecewise constants for fluxes. Applying our assumption that there is no flow in the direction tangent to control volume boundaries for piecewise linear pressures we get

$$\begin{aligned}
\|\nabla v\|_{L_2}^2 &= \int_\Omega (\nabla v)^2 dx \\
&= \sum_{l,n\in\omega} \int_{\gamma_{ln}} (\nabla v)^2 dx \\
&= \sum_{l,n\in\omega} \frac{1}{2}|\gamma_{ln}||Z_{ln}| \left[\left(\frac{v(x_n) - v(x_l)}{|Z_{ln}|} \right)^2 + \left(\frac{v(x_{\gamma_{ln}1}) - v(x_{\gamma_{ln}2})}{|\gamma_{ln}|} \right)^2 \right] \\
&= \sum_{l,n\in\omega} \frac{1}{2} \frac{|\gamma_{ln}|}{|Z_{ln}|} \left(v(x_n) - v(x_l)\right)^2;
\end{aligned}$$

the sizes $|Z_{ln}|$ and $|\gamma_{ln}|$ and points x_l and x_n are depicted on Figure 2, $x_{\gamma_{ln}1}$ and $x_{\gamma_{ln}2}$ are the endpoints of γ_{ln}, ω is the set of FE edges defining neighboring degrees of freedom. This expression is half of the square of our discrete norm introduced in (5.35). Since the solution to the continuous problem has continuous flux the integration in the derivation above is not exact and by the mean value theorem gives a value in some point in-between x_l and x_n so finally we have

$$\begin{aligned}
\|\nabla v\|_{L_2} &\leq \sqrt{\sum_{l,n\in\omega} \frac{1}{2}|\gamma_{ln}||Z_{ln}| \left(\frac{[v(x_n) - v(x_l)] + CH|Z_{ln}|}{|Z_{ln}|} \right)^2} \\
&\leq \sqrt{\sum_{l,n\in\omega} \frac{1}{2}|\gamma_{ln}||Z_{ln}| \left(\frac{[v(x_n) - v(x_l)] + CH^2}{|Z_{ln}|} \right)^2} \\
&\leq \sqrt{\sum_{l,n\in\omega} \frac{1}{2} \frac{|\gamma_{ln}|}{|Z_{ln}|} \left[\left(v(x_n) - v(x_l)\right)^2 + CH^4 \right]} \\
&\leq C|v|_{1,\bar{\Omega}^H} + CH.
\end{aligned}$$

The second part is to go the $\mathcal{H}^1$ norm from the seminorm which can be accomplished whenever we have a finite domain with zero Dirichlet boundary condition on

a part of the boundary using Friedrich's inequality (see, e.g., [9, page 30])

$$\left\|p^0 - p^H\right\|_{\mathcal{H}^1} \leq C \left|p^0 - p^H\right|_{L_2} \leq C|p^0 - p^H|_{1,\bar{\Omega}^H} + CH \leq CH \tag{5.47}$$

by corollary 5.14 and the derivation above. This fact can be written as a theorem.

THEOREM 5.15. *The coarse scale error is limited*

$$\left\|p^{0,h}_{MS} - p^{H,h}_{MS}\right\|_{\mathcal{H}^1} \leq CH. \tag{5.48}$$

6. Remarks on estimates for nonlinear flows. Due to the overall ellipticity of the problem, the results obtained in section 5 can be extended to weakly nonlinear flow in the sense where nonlinear terms are sufficiently small compared to the linear terms. In this regime, the resulting analysis retains the same structure, but becomes more involved as the propagation of fine-scale nonlinearities to the coarse scale needs careful attention. Since no new mathematical ideas are required, we choose to not present the rigorous proof, but only comment on the main aspects in section 6.1.

For nonlinear Navier–Stokes flow on the fine scale it is possible to show consistency of our method with the rigorously derived Dupuit–Forchheimer–Ergun law (see, e.g., [26, section 3.2.2]) which we show in section 6.2. However the error analysis for the multiscale discretization in the case of fully nonlinear flow is out of the scope of this paper, as it requires analysis for nonlinear control volume methods on the coarse scale.

6.1. Remark on an estimate for weakly nonlinear flows. We refer to weakly nonlinear problems in the sense that

- the solution on the fine scale is bounded by

$$\left|\frac{\mu}{\delta p_1}\vec{v}_i^{\epsilon} - \vec{u}_i\right| \leq \eta \tag{6.1}$$

  replacing (5.5) in the context of Lemma 5.3;
- the resulting problem maintains ellipticity properties as given in (5.39) and (5.15):

$$\tilde{B}v = \left(-\int_{\partial\tau_l} \vec{F}(\nabla v)\cdot\vec{n}_l ds\right)_{i\in I}, \tag{6.2}$$

$$\sum_{l\in I} v(x_l)(\tilde{B}v)_l \geq \gamma\,|v|^2_{1,\tilde{\Omega}^H}\,. \tag{6.3}$$

The nonlinearity constant η will influence the constant C in (5.4) and make the modeling error term in it (5.1) nonzero.

6.1.1. Changes in the proofs from section 5. Because of the ellipticity assumption (5.39) the structure used for estimates (5.2), (5.3) (Lemmas 5.13 and 5.7) will still be applicable. However, the proofs for several lemmas will be more technical, as linearizations must be introduced in several places.

As a representative example, in Lemma 5.13 in (5.40) before doing a linear splitting, the expression must be linearized to account for (6.1). This results in an additional factor of $(1+\eta)$ in the right-hand side of (5.46). However, as we assume η to be small, the factor can be treated as part of the constant C.

6.1.2. The modeling error for the case of weak nonlinearity. The deviation η due to nonlinearity introduced in (6.1) results in the following nonzero estimate for the modeling error,

$$\left\| p_0 - p_{MS}^{0,0} \right\|_{\mathcal{H}^1} \leq C\eta. \tag{6.4}$$

Here we summarize how it is derived.

The changes in the modeling error are caused by replacing Lemma 5.3 by assumption (6.1). The consequence is that in Theorem 5.6 using the nonlinearity bound in (5.11) will result in

$$max|\vec{v}_i^{Hom} - \vec{v}_i^{HMM}| \leq C\eta \tag{6.5}$$

replacing (6.1). This implies that in the worst case, if we linearize the problem in the HMM, the difference in data will be of order η and hence by the lemma analogous to 5.7 from the appendix the estimate for the modeling error takes the form of (6.4).

Remark 6.1. Even though for the nonlinear problem the estimate (6.4) becomes weaker than (5.1), it is important to remember that our benchmark solution obtained by homogenization is an approximation when $\varepsilon \to 0$. For problems with finite ϵ, the nonlinear behavior may be better captured by the HMM approach than by the homogenized solution.

6.2. Consistency with Dupuit–Forchheimer–Ergun law of fully nonlinear flow. In this section we highlight an additional result of our analysis with respect to fully nonlinear flow. In particular, the consistency of the method in terms of the homogenization result stated in Theorem 2.1 carries over to the homogenization result stated in Theorem 2.2. We directly infer that the method presented herein is consistent with the Dupuit–Forchheimer–Ergun law.

Here, refer back to the key components of the method and the homogenization result, recalling that the consistency of the method is preserved.

1. The only coarse scale equation in the system (2.8) (where fine scale is not present) is (2.8c). Coarse scale conservation for control volumes (3.1) is basically its conservative form with $\vec{F} = \vec{v}$.
2. As is shown in section 5.1.1 the pressure boundary conditions for our fine scale local problem are equivalent to imposing a pressure gradient as in (2.8a).
3. The fine scale part of DFE law ((2.8a) and (2.8b)) coincides with our fine scale cell problem (3.4).
4. Our data estimation operator $\vec{F}$ coincides with integration of flow over the fine scale domain given by (2.8f) as is shown in section 5.1.2.

The verification steps provided above are not sufficient to prove convergence for fully nonlinear case. While the full analysis of convergence for the fully nonlinear case is out of scope of this paper, we provide a numerical verification of convergence in section 7.3.

7. Numerical examples. In this section we present numerical examples that validate the properties of the CVHMMs discussed in this paper. In sections 7.1 and 7.2 we first emphasize the novelties presented in the paper, namely, the error estimate and different quadrature approximations. Thereafter we provide examples that illustrate capabilities of the method for cases where the theory was not fully developed. We extend theoretical results further in section 7.3 by an example illustrating convergence of the nonlinear solution to itself, supporting the consistency of the method

for nonlinear flows as discussed in section 6.2. After that, in section 7.4 we present a typical configuration of a heterogeneous domain for which nonlinear flows arise in applications. In the final example given in section 7.5, we explore how the presented method could be applied to nonsymmetric porous structures that lead to an effective anisotropic permeability field with nonzero off-diagonal components. In this last example the consistency of the coarse discretization is broken.

7.1. Comparison of error contributions. This numerical example verifies the rates of convergence proven in the error estimate (5.4). As this paper focuses mainly on the linear regime the results presented in this example only consider Stokes flow. For this case the theory in section 5 indicates the dependency of the error on the coarse and the fine scale grid resolutions (H and h) resulting from Theorems 5.15 and 5.9.

For our test we choose a simple problem on the unit square domain with zero Dirichlet boundary conditions and a forcing function with discontinuity, namely,

$$f = \begin{cases} \pi^2 \sin(\pi x)\sin(\pi y), & 0 \le x \le \frac{1}{2}, \quad 0 \le y \le 1, \\ 4\sin(\pi y) + \frac{1}{2}(-4x^2+4x)\sin(\pi y)\pi^2, & \frac{1}{2} \le x \le 1, \quad 0 \le y \le 1. \end{cases} \tag{7.1}$$

The pore structure is chosen to be homogeneous and isotropic; it is formed by circular grains with relative radius 0.4 forming a square arrangement. In the multiscale method the grains are approximated by polygons as on Figures 1(a)–(b).

We aim to compare our method to an analytical solution for the problem. As we are not aware of analytical solutions to the Stokes problem on this pore geometry, we use data estimation $a_{ap} = -F_{\|}(1)$ produced by our method on a very fine grid as a reference. With this approximation the problem will have a semianalytical homogenization solution of the form

$$\begin{cases} \frac{1}{2a_{ap}}\sin(\pi x)\sin(\pi y), & 0 \le x \le \frac{1}{2}, \quad 0 \le y \le 1, \\ \frac{1}{2a_{ap}}(-4x^2+4x)\sin(\pi y), & \frac{1}{2} \le x \le 1, \quad 0 \le y \le 1. \end{cases} \tag{7.2}$$

The discrete L_2 norms and $\mathcal{H}^1$ seminorms of error between the solution provided by the method and semianalytical solution (7.2) are plotted on Figure 5. The coarse unit square domain is initially a discretized regular grid with $H = 0.25$ and the fine scale cell problem has an unstructured triangulation as shown on Figure 1(b); h and H refinements are then performed uniformly on both scales. We first take a look at convergence rates. The rates of convergence proven in section 5 all concern the $\mathcal{H}^1$ norm.

Figure 5(c) indicate that the numerical solution converges in the $\mathcal{H}^1$ norm with rate H^2. This rate is higher than the predicted linear convergence in the estimate (5.4). The observed convergence rate in L_2 is also H^2 with respect to the coarse scale refinement. The fact that the convergence rates in both $\mathcal{H}^1$ and L_2 exceed the theoretical bound is typical for control volume methods on smooth problems (see, e.g., [23]).

The error due to propagation of the fine scale error can be studied from Figures 5(b) and 5(d). The cutoff on the rightmost point of the plots is a result of approximation of refinements reaching the resolution on which a_{ap} is approximated. The figures indicate that for considered porous media the rate of convergence is approximately h^2. This means that, as was noted in section 5.2.1 for our domain, $\alpha \approx 2$.

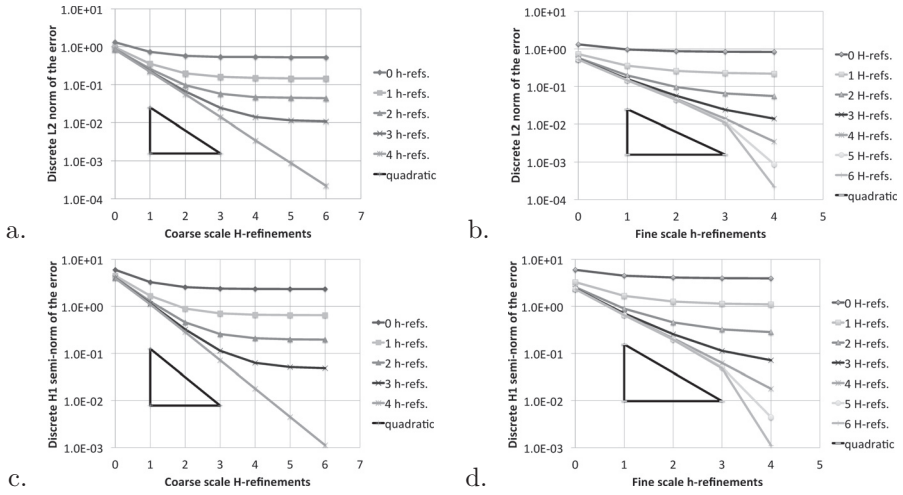

FIG. 5. *Discrete error norms for solutions with different levels of refinements plotted against coarse* (a), (c) *and fine* (b), (d) *grid sizes. All refinements are uniform and split the edges in half.*

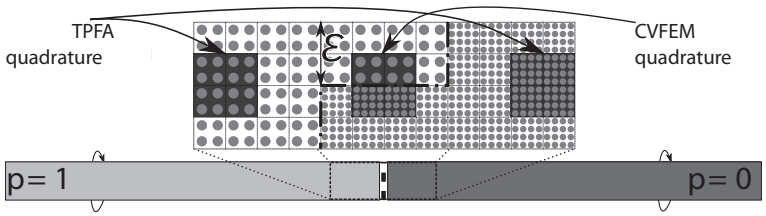

FIG. 6. *The structure of the domain with discontinuity with locations of quadrature points.*

The rate due to propagation of the fine scale error influences the errors in the H_1 and L_2 norms equivalently.

We conclude this example with emphasizing that no matter how fine either of the resolutions h or H is, the error may be governed by the other scale. The plateau on the upper plots on Figures 5 gives a good illustration. This fact is also important for single scale methods for which an effective parameter field is given: no matter how fine the resolution of the grid is, the real error may likely be dominated by the determination of the effective parameter.

7.2. Domain with a jump. In this example we address the issue discussed at the end of Remark 5.12. The industry standard for reservoir simulation is finite volume methods and the data that are provided by geologists contain grids for which the material discontinuities are resolved as closely as possible by the finite volume grid.

In this example we want to compare the two quadrature approximations introduced in section 3.3. As was mentioned in Remark 5.12, although TPFA style quadrature has a worse constant in the proof, it provides qualitative advantages when the discontinuity is resolved by the grid. To compare the two approaches we introduce an illustrative example that implements the situation depicted on Figure 4. As it is shown on Figure 6, the domain is chosen to be a stripe $1 \times 2\varepsilon$ with Dirichlet boundary

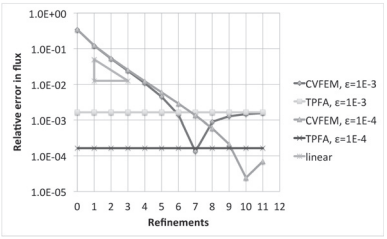

FIG. 7. *Relative error in flux compared to a problem with resolved discontinuity.*

conditions on left-right and periodic on top-bottom. Exactly in the middle of the domain a zigzag-shaped discontinuity is located; see Figure 6. The structure to the left of the discontinuity has a sparser pattern of the grains and hence higher permeability (around a factor of 20 contrast). Although our example is artificial, porous media with a contact zone between high- and low-permeable regions are common both in geological settings and in artificial porous media such as fuel cells and sanitation tissues.

Figure 7 presents the comparison of relative error in flux between the two strategies to choose quadrature on a relatively sparse grid compared to a solution that resolves the configuration of the quadrature. The domain initially has four degrees of freedom distributed evenly along the $1 \times 2\varepsilon$ strip that is doubled with each refinement. The figure illustrates that although CVFEM-style approximation converges to the solution with the expected rate before having stagnation near the asymptote, TPFA-type quadrature achieves that asymptotic accuracy already for the coarsest grid and maintains it. The errors for both methods will fall below the asymptotic accuracy when the structure of the discontinuity is resolved.

The reason for the poor approximation properties of CVFEM for coarse grids is that it uses a flux approximation that is close to an arithmetic mean around the discontinuity for the given setup and is not stable with respect to perturbations in general (see Figure 4(a)). This leads to overestimation of the flux for low grid resolutions, as opposed to TPFA that provides a harmonic mean, hence underestimating slightly the true behavior. The kink towards zero in the error for CVFEM-type method is due to change of sign in the approximation. Overestimation for the arithmetic means changes to underestimation because the cell problem located in the discontinuity region returns an underestimated value of permeability of about 21% emphasizing again the sensitivity to the small perturbation of the quadrature point location even for idealized cases as on Figure 6. For flows across discontinuities, the correct effective property in the limit is the harmonic mean (see, e.g., [2]) that is one of the reasons for TPFA-type methods becoming standard in reservoir simulation.

This example emphasizes that while the error of CVFEM-style method for a grid with a resolved discontinuity converges with a theoretically expected rate of H, the TPFA-style quadrature resolves the macroscopic discontinuity, and its error is proportional to "thickness" of discontinuity 2ε.

7.3. Convergence of nonlinear flow to itself. In section 6.2 the consistency between the proposed CVHMM and nonlinear homogenization was shown. In this example we provide numerical indication that verifies convergence of the method for the nonlinear case.

In absence of analytical solutions for Dupuit–Forchheimer–Ergun flows, in this example we test all solutions against a numerical solution computed on very fine grids

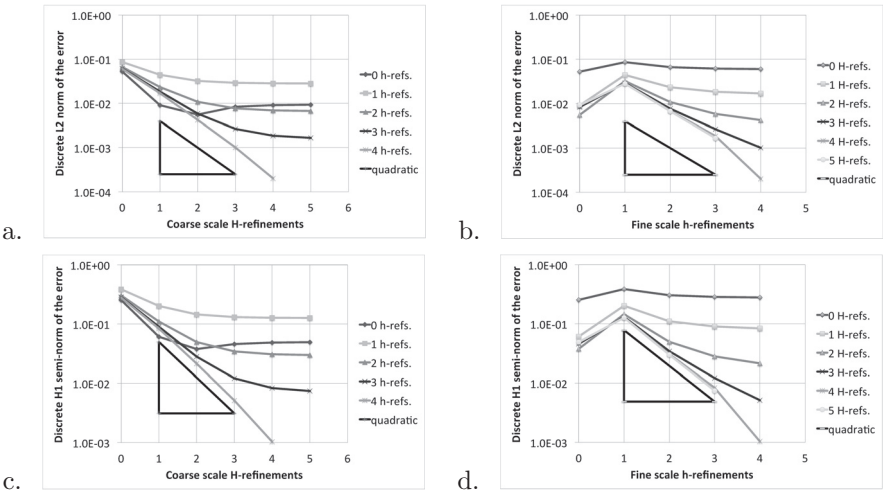

FIG. 8. *Discrete error norms for nonlinear solutions with different levels of refinements plotted against coarse* (a), (c) *and fine* (b), (d) *grid sizes.*

on both scales. The problem setup is analogous to section 7.1. The difference is that on the fine scale a fully nonlinear cell problem is used with $\mu = 0.004$ (Problem 3.2) and the starting grid is one level coarser than the grid used for the linear case (see Figure 1(b)). With these parameters the discrepancy between the solution to the full nonlinearity coarse scale flux as compared to the linearized flow is up to 20%.

The discrete error norms of solutions to the nonlinear problem compared to a reference solution on detailed coarse and fine grids is presented on Figure 8. Comparing convergence plots the for nonlinear problem (Figure 8) to those verifying linear convergence (Figure 5) illustrates that the nonlinear problem converges with the same rates with respect to both fine and coarse scale refinements. As it was observed in section 7.1 for the linear case, the errors are of order $(\frac{h}{\varepsilon})^2$ and H^2, respectively, for both norms. This gives a good indication of the robustness of the method in the nonlinear regime for which analytical results are not obtained.

7.4. Features of nonlinear flow in heterogeneous medium. One of the strong points of our method remains its flexibility with respect to the choice of the fine scale problem. While the focus of this paper is analysis of convergence of the CVHMM for the linear case, it is important to point out its applicability outside convergence theory.

This numerical example shows all the potential of our method and indicates problems for which nonlinearities play a crucial role. We consider a nonlinear flow problem (induced by full Problem 3.2 with $\mu = 0.04$) on a heterogeneous domain composed of regions made out of cells illustrated on Figures 1(b) and 1(c) combined in an altering frame manner as shown on the bottom of Figure 9(a). The part composed of grid cells of Figure 1(b)-type gives an anisotropic region which is approximately 4 times less permeable than the isotropic region composed of the Figure 1(c)-type cells. The boundary conditions are no-flow for all outer boundaries of the domain except for one sink that is represented by the zero Dirichlet boundary condition located in the left middle on the side of the low-permeable region. The flow is driven by the load function that is nonzero in one grid point on the opposing boundary in the

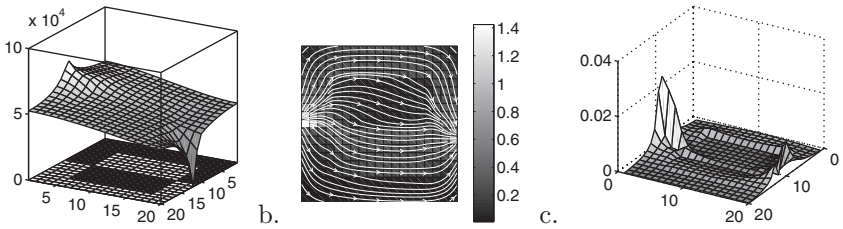

FIG. 9. *Pressure solution to nonlinear problem plotted over the domain schematics (light indicate heterogeneous low-permeable areas)* (a), *corresponding flow solution* (b), *and special distribution of nonlinear effects* (c).

high-permeable region, simulating a source well. To handle discontinuities correctly TPFA-type quadrature is used for sampling.

The pressure and the flow solutions to the described nonlinear problem are depicted on Figures 9(a) and 9(b), respectively. As expected most of the flow is driven along the high-permeable frame part and there are pressure buildups near the source and the sink. The latter one is larger due to lower permeability.

Another purpose of this example is to identify regions where nonlinearity is most crucial for a heterogeneous domain. Figure 9 shows the the modulus of difference between linear and nonlinear solutions in different parts of the domain. It is no surprise that the nonlinearity is biggest for parts with highest flow velocity; that is, first of all, point sources and sinks. In the rest of the domain nonlinear effects are generally larger in high-permeable areas. Moreover there is noticeable focusing effects on the outer corners of the low-permeable region in the center.

7.5. Application to nonsymmetric porous structures. It is well known that for general porous structures and, as a result, for general permeability fields two point methods including the methodology described in the current paper, are not consistent and therefore converge to the wrong solution (see, e.g., [3]). However, for the majority of geological applications the anisotropy is aligned with the grid to the extent that the consistency error is acceptable. Therefore TPFA remains standard in industrial reservoir simulation (such as the Eclipse software by Schlumberger). TPFA leads to linear systems that are M-matrices, which in turn guarantees monotonicity of the fluid potential and a physically reasonable solution. For the cases when the structure is not aligned with the grid there exist several methods to overcome those constraints including perturbing the grid so it is K-orthogonal and a TPVA is valid (see, e.g., [1]), modifying positions of collocation points in two-point flux scheme forming a nonlinear problem (see, e.g., [30]) or using a multipoint flux approximation (see, e.g., [2]). While the methods described above are out of the scope of this paper, here we present an example indicating that for randomly generated grain structure (as on Figure 10(a)) the errors decrease to a certain point before being limited by the consistency error of the coarse grid.

For this example we consider a coarse linear problem of the type

$$-\nabla \cdot A\nabla p = f \tag{7.3}$$

solved on the unit square, for which A is computed from solving homogenization cell problems numerically for the cell from Figure 10(a) on a refined grid. The f is than

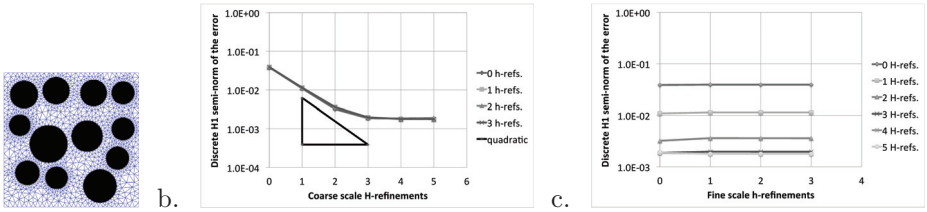

FIG. 10. *An example of randomly generated anisotropic porous structure* (a) *and discrete error norms for solutions for domain composed of those for different levels of refinements plotted against coarse* (b) *and fine* (c) *grid sizes.*

computed from (7.3) by substituting

$$p = (0.5 - |x - 0.5|)\,(0.5 - |y - 0.5|)\,. \tag{7.4}$$

The comparison of the numerical results for different grid resolutions to the solution (7.4) in discrete norms is presented on Figure 10. Here, as earlier, we start out with $H = 0.25$ on the coarse scale and grid depicted on Figure 10(a) and then perform uniform refinements.

Figure 10(b) shows expected rate of convergence for the first refinements of the coarse grid, after which the error due to lack of consistency dominates. In this example fine scale grid refinement does not provide any improvement as the error due to off-diagonal components, that is not accounted for, dominates over the propagation of fine scale error (see Figure 10(c)).

This last example provides an alternative view of our method. The TPFA discretization chosen for the coarse grid is considered sufficiently accurate for a broad range of industrial applications. We may thus choose to consider the consistency error as a sufficient tolerance for the multiscale algorithm from a practical viewpoint. This view allows us to interpret that for the current example, even the coarsest fine scale solver is sufficient to obtain the accuracy needed in practical applications.

8. Conclusions. In this paper we have presented a heterogeneous multiscale method for modeling flow in porous media taking explicitly into account pore scale equations. The method presumes only the continuity equation on the coarse scale and the pressure-flow relationship is numerically derived by solving problems on fine scale geometry locally. The presented implementation of the method permits both Stokes and steady state Navier–Stokes equations on the fine scale. Thus both linear and non-linear coarse scale pressure-flow relations can be modeled by this approach. Two possible choices of quadrature points for the reconstruction of the coarse scale flux were presented. Those choices result in HMMs that generalize the CVFEM and finite difference method with TPVA. HMMs with the latter choice of quadrature had not been analyzed in previous works.

The particular focus of this paper has been the convergence analysis of the presented HMM. For methods in which scales differ significantly, a reconstruction of the full fine scale solution is not important. By a comparison with the homogenization solution of the Stokes problem, we proved an a priori error estimate for the coarse scale pressure in the case of linear flow. The estimate is done in the $\mathcal{H}^1$ norm that also implies the estimate on the coarse flux. It is shown that the error can be split into three parts: a modeling error which is zero when the flow is linear, a term proportional to the size of the coarse grid, and a term that is dependent on the fine scale geometry, grid size, and the size of the fine scale problems. We also discussed the extension of

the proof to the weakly nonlinear case, for which the modeling error is no longer zero as well as consistent with a more complicated Dupuit–Forchheimer–Ergun law for the fully nonlinear case.

Numerical results provided in the paper verify the estimate and emphasize the importance of appropriate accuracy on both the coarse and fine scales. They also indicate similar convergence behavior for nonlinear problem. We also provide an example comparing different choices of quadrature on domains with coarse discontinuity. Moreover for heterogeneous domain with discontinuity we identify some typical regions for which nonlinearities have marked influence.

Acknowledgments. We want to thank Jörg Willems from Johann Radon Institute for Computational and Applied Mathematics, Annette Stephansen from CMR, as well as Henrik Kalisch and Florin Radu from the University of Bergen for helpful discussion and references.

REFERENCES

[1] I. Aavatsmark, *Interpretation of a two-point flux stencil for skew parallelogram grids*, Comput. Geosci., 11 (2007), pp. 199–206.

[2] I. Aavatsmark, *Multipoint flux approximation methods for quadrilateral grids*, in The 9th International Forum on Reservoir Simulation, Abu Dhabi, United Arab Emirates, 2007, pp. 9–13.

[3] I. Aavatsmark, T. Barkve, Ø. Bøe, and T. Mannseth, *Discretization on non-orthogonal, quadrilateral grids for inhomogeneous, anisotropic media*, J. Comput. Phys., 127 (1996), pp. 2–14.

[4] A. Abdulle, *On a priori error analysis of fully discrete heterogeneous multiscale FEM*, Multiscale Model. Simulation, 4 (2005), pp. 447–459.

[5] A. Abdulle, *The finite element heterogeneous multiscale method: A computational strategy for multiscale PDEs*, in Multiple Scales Problems in Biomathematics, Mechanics, Physics and Numerics, Math. Sci. Appl., 31 (2009), pp. 133–181.

[6] A. Abdulle and W. E, *Finite difference heterogeneous multi-scale method for homogenization problems*, J. Comput. Phys., 191 (2003), pp. 18–39.

[7] G. Allaire, *One-phase Newtonian flow*, in Homogenization and Porous Media, U. Hornung, ed., Springer, New York, 1996, pp. 45–68.

[8] S. Alyaev, E. Keilegavlen, and J. M. Nordbotten, *Multiscale simulation of non-Darcy flows*, in Computational Methods in Water Resources XIX, Urbana-Champaign, IL, 2012, pp. 1–8.

[9] D. Braess, *Finite Elements: Theory, Fast Solvers, and Applications in Solid Mechanics*, Cambridge University Press, Cambridge, 2007.

[10] A. Brandt, *Multiscale scientific computation: Review* 2001, in Multiscale and Multiresolution Methods, Lecture Notes Comput. Sci. Eng. 20, Springer, Berlin, 2002, pp. 3–95.

[11] H. C. Brinkman, *A calculation of the viscous force exerted by a flowing fluid on a dense swarm of particles*, Appl. Sci. Res. Sect. A, 1 (1947), pp. 27–34.

[12] Z. Cai, J. Mandel, and S. McCormick, *The finite volume element method for diffusion equations on general triangulations*, SIAM J. Numer. Anal., 28 (1991), pp. 392–402.

[13] Z. Chen, *On the heterogeneous multiscale method with various macroscopic solvers*, Nonlinear Anal., 71 (2009), pp. 3267–3282.

[14] Z. Chen, S. L. Lyons, and G. Qin, *Derivation of the Forchheimer law via homogenization*, Transp. Porous Media, 44 (2001), pp. 325–335.

[15] J. Chu, B. Engquist, M. Prodanovi, and R. Tsai, *Advances in Applied Mathematics, Modeling, and Computational Science*, Fields Institute Comm. 66, Springer, Boston, 2013.

[16] J. Chu, B. Engquist, M. Prodanovic, and R. Tsai, *A multiscale method coupling network and continuum models in porous media* I: *Steady-state single phase flow*, Multiscale Model. Simulation, 10 (2012), pp. 515–549.

[17] L. J. Durlofsky, *Numerical calculation of equivalent grid block permeability tensors for heterogeneous porous media*, Water Res. Res., 27 (1991), pp. 699–708.

[18] W. E, *The Heterogeneous Multiscale Method and the "Equation-free" Approach to Multiscale Modeling*, Multiscale Modeling, https://web.math.princeton.edu/~weinan/pdf%20files/HMM-eqfree.pdf (2011).

[19] W. E and B. Engquist, *The heterogeneous multiscale methods*, Comm. Math. Sci., 1 (2003), pp. 87–132.
[20] W. E, B. Engquist, X. Li, W. Ren, and E. Vanden-eijnden, *Heterogeneous multiscale methods: A review*, Comm. Comput. Phys., 2 (2007), pp. 367–450.
[21] W. E, P. Ming, and P. Zhang, *Analysis of the heterogeneous multiscale method for elliptic homogenization problems*, J. Amer. Math. Soc., 18 (2005), pp. 121–156.
[22] Y. Efendiev and T. Hou, *Multiscale finite element methods for porous media flows and their applications*, Appl. Numer. Math., 57 (2007), pp. 577–596.
[23] G. T. Eigestad and R. A. Klausen, *On the convergence of the multi-point flux approximation o-method: Numerical experiments for discontinuous permeability*, Numer. Methods Partial Differential Equations, 21 (2005), pp. 1079–1098.
[24] V. Girault and P.-A. Raviart, *Finite Element Methods for Navier-Stokes Equations Theory and Algorithms*, Springer-Verlag, Berlin, 1986.
[25] S. Majid Hassanizadeh and W. G. Gray, *Thermodynamic basis of capillary pressure in porous media*, Water Res. Res., 29 (1993), pp. 3389–3405.
[26] U. Hornung, *Homogenization and Porous Media*, Interdiscip. Appl. Math. 6, Springer Verlag, New York, 1997.
[27] M. K. Hubbert, *The theory of ground-water motion*, J. Geol., (1940), pp. 785–944.
[28] V. Kippe, J. E. Aarnes, and K.-A. Lie, *A comparison of multiscale methods for elliptic problems in porous media flow*, Comput. Geosci., 12 (2008), pp. 377–398.
[29] J. Li, P. G. Kevrekidis, C. W. Gear, and I. G. Kevrekidis, *Deciding the nature of the coarse equation through microscopic simulations: The baby-bathwater scheme*, SIAM Rev., 49 (2007), pp. 469–487.
[30] K. Lipnikov, M. Shashkov, D. Svyatskiy, and Y. Vassilevski, *Monotone finite volume schemes for diffusion equations on unstructured triangular and shape-regular polygonal meshes*, J. Comput. Phys., 227 (2007), pp. 492–512.
[31] A. Logg, K. A. Mardal, and G. N. Wells, *Automated Solution of Differential Equations by the Finite Element Method*, Lecture Notes Comput. Sci. Eng. 84, Springer, Berlin, 2012.
[32] I. Lunati and P. Jenny, *Multiscale finite-volume method for compressible multiphase flow in porous media*, J. Comput. Phys., 216 (2006), pp. 616–636.
[33] A. Quarteroni and A. Valli, *Numerical Approximation of Partial Differential Equations*, Springer Ser. Comput. Math. 23, Springer Verlag, Berlin, 1997.
[34] A. Tamayol and M. Bahrami, *Analytical determination of viscous permeability of fibrous porous media*, Internat. J. Heat Mass Transfer, 52 (2009), pp. 2407–2414.
[35] R. Verfürth, *Error estimates for a mixed finite element approximation of the Stokes equations*, RAIRO. Anal. Numér., 18 (1984), pp. 175–182.
[36] S. Whitaker, *Advances in theory of fluid motion in porous media*, Indust. Engrg. Chem., 61 (1969), pp. 14–28.
[37] X. Yue and W. E, *Numerical methods for multiscale transport equations and application to two-phase porous media flow*, J. Comput. Phys., 210 (2005), pp. 656–675.